IOP Publishing Journal of Physics G: Nuclear and Particle Physics
J. Phys. G: Nucl. Part. Phys. **47** (2020) 045005 (21pp) https://doi.org/10.1088/1361-6471/ab6948

Collider signature of U_1 Leptoquark and constraints from $b \to c$ observables

Aritra Biswas, Dilip Kumar Ghosh, Nivedita Ghosh, Avirup Shaw and Abhaya Kumar Swain[1]

School of Physical Sciences, Indian Association for the Cultivation of Science, 2A & 2B Raja S.C. Mullick Road, Jadavpur, Kolkata 700 032, India

E-mail: iluvnpur@gmail.com, tpdkg@iacs.res.in, tpng@iacs.res.in, avirup.cu@gmail.com and abhayakumarswain53@gmail.com

Received 4 November 2019, revised 3 January 2020
Accepted for publication 8 January 2020
Published 5 March 2020

Abstract

One of the most popular models that is known to be able to solve the lepton flavour universality violating charged ($b \to c$) and neutral current ($b \to s$) anomalies is the Leptoquark Model. In this work we examine the *multijet* + $\not{E}_T$ collider signature of a vector leptoquark (U_1) which has the potential to mediate both the charged and neutral current processes at tree level. From our collider analysis we derive the exclusion limits on mass for the U_1 leptoquark at 95% C.L. at the current and future experiment of the Large Hadron Collider. We also calculate the effect of such a leptoquark in $b \to c$ observables.

Keywords: beyond the SM, leptoquarks, B physics, collider physics

(Some figures may appear in colour only in the online journal)

1. Introduction

The Standard Model (SM) of particle physics is the most successful theoretical description of the experimentally detected spectrum of fundamental particles till date. This description is based on the gauge invariance of the local group $SU(3)_C \times SU(2)_L \times U(1)_Y$. The quarks and leptons enter this description as independent fields. However, the success of the SM as a quantum field theory is crucially dependent on the cancellation between the lepton and quark contributions to triangle anomalies of gauged currents. As such, it is only logical to expect that a more fundamental description of these particles might incorporate an interrelation between the quarks and the leptons [1].

[1] Author to whom any correspondence should be addressed.

The Leptoquark (or Lepto-quark) (LQ) is such an extension of the SM where the LQs are hypothetical particles which mediate interactions between quarks and leptons at tree-level. Such scenarios emerge naturally in several extensions of the SM (e.g. composite models [2], Grand Unified Theories [3–10], superstring-inspired E_6 models [11–14] etc). The discovery of LQs would thus be a signal for matter unification. As such, these particles have extensively been discussed theoretically for over forty years, both from the point of view of their diverse phenomenological aspects [15–17], and specific properties [18–20, 1, 21–39]. A considerable amount of work regarding LQs has also been undertaken from the experimental side. However, the major part of these searches have been directed towards scalar LQs [40–44]. Experimental studies on vector LQs, though present in the literature [45–47], are scarce in number mainly because of some additional model dependent parameters.

On a different note, there have been constant and consistent hints towards the presence of lepton flavour universality violating (LFUV) new physics (NP) both in charged-current [48–53] and neutral-current [54–56] processes over the last few years. These flavour anomalies exhibit diverse phenomenological roles in validating/invalidating or constraining a plethora of existing NP models. Various versions of LQ models have also been used in explaining these anomalies [57–60, 34, 61–70]. The advantage in doing so is that LQ is one of those few models which allows for all the different kinds of NP interactions (based on their Lorentz structures, viz scalar, pseudo-scalar, vector, axial-vector and tensor) that have the potential to explain such deviations. If LQs are potential candidates for explaining such anomalies, it is imperative that one carefully investigates the production and decay signatures of these entities at collider experiments and predict observables which help in their detection. As a result, the phenomenological community has recently displayed a lot of interest in collider studies of LQs [24–26, 28, 31, 32, 71, 72, 45, 73, 46, 74]. However, collider searches dedicated to vector LQs in particular are very limited in the literature [45, 28, 74, 73, 46].

In the present article, we choose a particular vector LQ U_1 which is among those few LQs that, in the most general case (i.e. with couplings to all three generations of fermion) has the potential to explain the data of both neutral current (e.g. $\mathcal{R}_{K^{(*)}}$) and the charged current (e.g. $\mathcal{R}_{D^{(*)}}$) anomalies. However, the most recent data on $\mathcal{R}_{D^{(*)}}$ due to Belle [75] has brought the global deviation for these ratios with respect to SM down from $\sim 4\sigma$ to $\sim 3.1\sigma$. This, in principle, should result in even tighter constraints for the allowed parameter space corresponding to the U_1 vector LQ model. With this spirit, we propose a scenario where the U_1 vector LQ can couple with second and third generations of quarks but with only third generation of leptons. Therefore, the parameter space for the variant of the model discussed in the current article will not be affected by the $\mathcal{R}_{K^{(*)}}$ observables. However, the implications of the $\mathcal{R}_{D^{(*)}}$ ratios will result in a constrained parameter space, which has also been looked into in the scope of this article. Further, this LQ has baryon and lepton number conserving couplings. Consequently, there is no possibility of proton decay being mediated by U_1[2]. On top of that, the NP interaction term that imparts to the $\mathcal{R}_{D^{(*)}}$ observable will also contribute to the production of di-top plus missing energy. In this set up we perform a comprehensive collider analysis of U_1 vector LQ via *multijet* + $\not{E}_T$ final states. We have utilized several interesting kinematic variables which best exploit the available kinematic information between the signal and background events to maximize the collider reach for 13 TeV LHC. Our analysis shows that the U_1 vector LQ can be excluded up to 2020 (2230) GeV at 95% C.L. for an integrated luminosity of 300 (3000) fb^{-1}. After obtaining the bound on the mass of the U_1 vector LQ from the collider analysis, we hence incorporate the

[2] At this point we remark in passing that, the lepton and baryon number violating LQs are very heavy in order to avoid bounds from proton decay. However, the LQs with the baryon and lepton number conserving couplings restrict proton decay and could be light enough to be seen in the LHC [76].

corresponding flavour analysis to provide a quantitative estimate of how well this present version of the U_1 vector LQ model describes the current $b \to c$ data.

The paper is organised as follows. We briefly describe the Lagrangian for the U_1 vector LQ and set our convention in section 2. Section 3 we perform the collider analysis for U_1 via *multijet* + $\not{E}_T$ final states. In section 4 we study the $b \to c$ observables mediated by the U_1 vector LQ. Finally, we summarize our results in section 5.

2. Effective Lagrangian of U_1 vector Leptoquark

It has been already mentioned that, LQs are special particles that appear naturally in particular extensions of the SM. Depending on the considered model, the LQs may be scalar (spin 0) or vector (spin 1) particles. All the LQs are colour-triplet and carry both baryon as well as lepton numbers. As a consequence they are able to mediate transitions between the quark and lepton sectors. Apart from the SM particles, a general LQ model[3] contains at least two massive neutrinos and twelve LQ particles. Among the twelve LQs, six are scalars (S_3, R_2, $\tilde{R}_2$, $\tilde{S}_1$, S_1, $\bar{S}_1$) and the rest (U_3, V_2, $\tilde{V}_2$, $\tilde{U}_1$, U_1, $\bar{U}_1$) transform vectorially under Lorentz transformations. As discussed earlier, the focus for the rest of our article will be on U_1 vector LQ. The Lagrangian for kinetic and mass terms of U_1 vector LQ is given by [73]:

$$\mathcal{L}^1_{U_1} = -\frac{1}{2}U^\dagger_{\mu\nu}U_{\mu\nu} - ig_s\kappa\ U^\dagger_{1\mu}T^a U_{1\nu}G^a_{\mu\nu} + m^2_{U_1}U^\dagger_{1\mu}U_{1\mu}, \tag{1}$$

where m_{U_1} denotes the mass of U_1 vector LQ. κ is a dimensionless coupling that depends on the ultraviolet origin of the vector [73]. For the minimal coupling case $\kappa = 0$, while for the Yang–Mills case $\kappa = 1$ [73]. Throughout our analysis we have assumed $\kappa = 1$. $U_{\mu\nu} = D_\mu U_{1\nu} - D_\nu U_{1\mu}$ is a field strength tensor. $G^a_{\mu\nu}$ is the gluon field strength tensor, T^a is the Gell–Mann matrix and g_s is the QCD coupling strength. Generically, the Yukawa Lagrangian of the U_1 with the SM fermion bilinear can be written as [76]:

$$\mathcal{L}^2_{U_1} = (h^{ij}_{1L}\bar{Q}_{iL}\gamma^\mu L_{jL} + h^{ij}_{1R}\bar{d}_{iR}\gamma^\mu l_{jR})U_{1\mu} + \text{h.c}\,.. \tag{2}$$

The gauge quantum numbers for U_1 under the SM gauge group $SU(3)_C \times SU(2)_L \times U(1)_Y$ are $(\mathbf{3}, \mathbf{1}, \frac{2}{3})$. $Q^T_L \equiv (u\ \ d)$ denotes the left handed quark doublet, $L^T_L \equiv (\nu_l\ \ l)$ stands for the left handed lepton doublet, d_R is the right handed down type quark singlet and l_R represents the right handed charged lepton. $h^{ij}_{1L(R)}$ are the left (right) handed Yukawa coupling constants while $i, j \equiv 1, 2, 3$ specify the fermion generation indices.

3. Collider analysis

We begin our collider analysis by specifying the signal topology that we consider:

$$pp \to U_1\overline{U_1} \to (t\ \bar{\nu}) + (\bar{t}\ \nu), \tag{3}$$

where the $\overline{U_1}$ represents the anti-particle of the U_1 vector LQ. The interaction term responsible for the pair production of the U_1 vector LQ at the LHC is given in the Lagrangian $\mathcal{L}^1_{U_1}$ (see equation (1)). The Feynman diagrams for the pair production of the U_1 vector LQ given in the left panel of figure 1. The signal in equation (3) is characterized by the presence of di-top and large missing energy ($\not{E}_T$) in the final state which we designated as di-top signal. We have assumed here that the U_1 vector LQ couples only to the third generation quarks and leptons by

[3] For detailed discussions regarding LQ scenarios, one can look into [76].

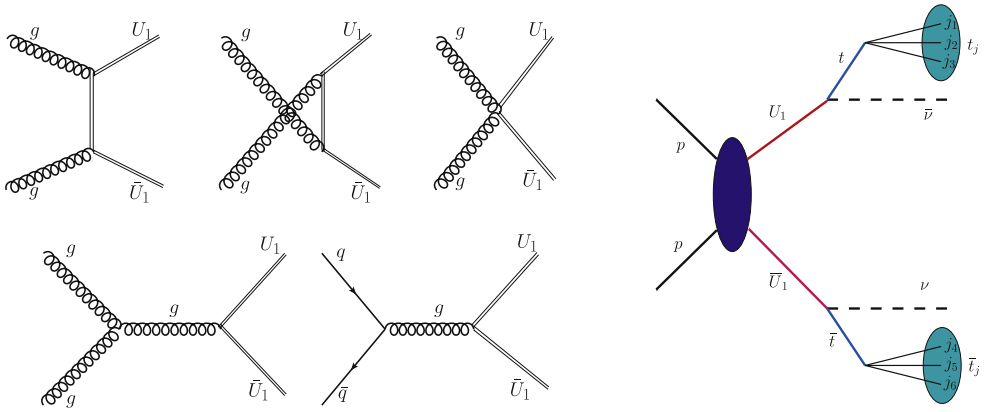

Figure 1. (Left) panel displays the Feynman diagrams which contribute the U_1 vector LQ pair production. (Right) panel is a representative kinematic diagram for the pair production of the U_1 vector LQ, each of which subsequently decays to the top quark and neutrino. The top (anti-top) quark further decays hadronically leading to multijets and missing energy in the final state. Since the top (anti-top) is produced from the U_1 vector LQ, it is highly boosted and hence the decays are collimated. The collimated objects are diagrammatically represented as green blobs. The black dashed lines represent the neutrinos which are undetected in the detector and give rise to momentum imbalance, viz the missing transverse momenta.

assigning non-zero values to the corresponding couplings while setting the other couplings to zero. Furthermore, we also consider the coupling of U_1 to top quark and neutrino to be equal to that of the bottom and tau-lepton in order to simplify[4] our analysis. Therefore, the branching ratio for each channel is approximately 50%. Each top quark in the final state is assumed to decay hadronically. Since the top quark is produced from the (very heavy) U_1 vector LQ, it is expected to have large boost. The corresponding decays are hence collimated and fall inside a large radius jet (marked by green blobs in the right panel of figure 1) which is discussed below. Therefore, we expect at least two large radius jets, N_{fatJet}, with transverse momentum (P_T) $>$ 50 GeV and large missing transverse energy ($\not{E}_T$ $>$ 100 GeV). Since the signal has multijets in the final state, we further demand that there should at least be two jets in the final state with $P_T^j \geqslant 20$ GeV and $|\eta_j| \leqslant 2.4$ and the reconstructed leptons (electrons and muons) with $P_T^l \geqslant 10$ GeV and $|\eta_l| \leqslant 2.4$ are vetoed.

The SM processes which contribute as backgrounds to the above final state are $t\bar{t}$ + jets, V+ jets, where $V = W^{\pm}$, Z and QCD multijets (up to four jets). Since the QCD multijets have very small missing transverse energy, it can be handled using a moderate to large missing energy cut, so the dominant contribution comes from the top pair events and V+ jets backgrounds. The signal significance can be maximized subject to appropriate choices for the kinematic variables. The events corresponding to the signal and SM backgrounds in our analysis have been generated using `Madgraph5` [77] with the `NNPDF3.0` parton distribution functions [78]. The UFO model files required for the Madgraph analysis have been obtained from `FeynRules` [79] after a proper implementation of the model. Following this parton level analysis, the parton showering and hadronisation are performed using `Pythia` [80]. We use `Delphes`(v3) [81] for the

[4] However, a more general analysis can be done using different values for the couplings. Such an analysis can potentially provide limits in coupling-mass plane. We, however, choose to make the analysis as simple as possible by reducing free parameters of the model.

corresponding detector level simulation after the showering/hadronisation. The jet construction at this level has been performed using fastjet [82] which involves the anti-K_T jet algorithm with radius $R = 0.5$ and $P_T > 20$GeV. The hard-jet background as well as the signal events have been properly matched using the MLM matching scheme [83]. The signal and backgrounds except $V+$ jets are matched up to 2 jets and matching for $V+$ jets are done up to 4 jets. After getting the reconstructed jets in each event, we again pass the jets through the fastjet with radius[5] $R = 0.8$ to get the large radius jets with $P_T > 50$GeV for the di-top signal.

The cross section used in this analysis for the background process $t\bar{t}$ is 815.96 pb [84] as calculated with the Top++2.0 program to NNLO in perturbative QCD, with soft-gluon resummation to NNLL order assuming a top quark mass of 173.2 GeV. The single vector boson production cross section used in this analysis is 6.18×10^4 pb (1.979×10^4 pb) for $W^{\pm}+$ jets ($Z+$ jets)[6] at NNLO. Finally, the cross section for QCD multijets backgrounds are taken from the Madgraph. For the signal, we have used the LO cross section calculated from the Madgraph to give a conservative collider reach.

The signal topology as in equation (3) is shown in the right panel of figure 1 where each U_1 vector LQ decays to the top quark and anti-neutrino. Subsequently, the top quark decays hadronically and the decay products are collimated because they are produced from a highly boosted top quark. The deep green blobs are diagrammatic representation of the large radius jets denoted as t_j ($\bar{t}_j$) from the top (anti-top).

Several kinematic variables have been used in our analysis which utilize the available kinematic information to maximize the significance. They are: missing transverse energy ($\not{E}_T$), transverse mass variable M_{T2} [85–94], $\sqrt{\hat{s}}_{\min}$ [95–100], razor variables [101–104], H_T [105] and M_{eff} [106] which we discuss briefly in what follows.

The missing transverse energy, $\not{E}_T$, is the momentum imbalance in the transverse direction. It is expected to have a significant value subject to the presence of invisible particles in the final state. Otherwise, it attains a comparatively smaller non-zero value owing to mismeasurement. Since the signal considered here has neutrinos in the final state, they generate a significant amount of missing energy. The missing energy corresponding to the background events, however, is mostly due to mismeasurement except for some small fraction of events where neutrinos contribute. Figure 2, (left panel) shows the distribution of missing transverse energy for signal and backgrounds where the red colour corresponds to signal and only the dominant backgrounds are displayed. The mass of the U_1 vector LQ in this representative plot is taken to be 1 TeV. One can immediately verify that $\not{E}_T$ for the signal peaks at a value that is much higher compared to the backgrounds where it peaks at values close to zero. Hence, $\not{E}_T$ is an important variable suitable for handling the large SM backgrounds.

The mass bound variable $\sqrt{\hat{s}}_{\min}$ [95–100] has been proposed to measure the mass scale associated with NP. This is a global and inclusive variable which can be applied for any event topology without caring about the number of parent and the number of invisible particles involved in the topology. When there are invisible particles present in the final state, it is very challenging to get the information of the partonic center of momentum (CM) energy, $\sqrt{\hat{s}}$, which is nothing but the mass of the heavy resonance for singly production or the threshold of the pair production. $\sqrt{\hat{s}}_{\min}$ is an interesting way out where the peak (end-point) of the distribution is nicely correlated with the pair production (singly produced heavy resonance). For a given event, it is defined as the minimum partonic CM energy that is required to

[5] Since the top will be highly boosted, the top decay products will fall in the large radius jets of radius of 0.8 on a statistical basis and we have also checked that changing the jet radius will have a mild effect on the results presented here.

[6] Measurement of the Production Cross sections of a Z Boson in Association with Jets in pp collisions at $\sqrt{s} = 13$ TeV with the ATLAS Detector, Tech. Rep. ATLAS-CONF-2015-041, CERN, Geneva, Aug, 2015.

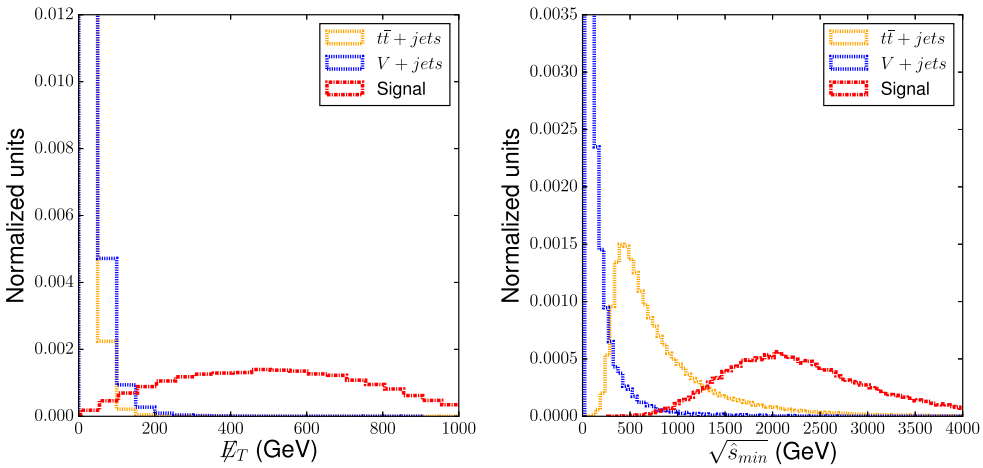

Figure 2. The variable missing transverse energy (left panel) and $\sqrt{\hat{s}}_{\rm min}$ (right panel) are displayed here. The signal, in red colour, here corresponds to the pair production of the U_1 vector LQ with mass 1 TeV. The dominant backgrounds, $t\bar{t} + jets$, $V + jets$ with $V = W^{\pm}/Z$ are displayed in orange and blue, respectively.

produce the given final state particles and the measured missing transverse energy. Mathematically

$$\sqrt{\hat{s}_{\rm min}(m_{inv})} = \sqrt{(E^{vis})^2 - (P_z^{vis})^2} + \sqrt{\vec{\not{P}}_T^{\,2} + m_{inv}^2}, \tag{4}$$

where m_{inv} is sum of the invisible particle masses while $E^{vis} = \sum_j e_j^{vis}$ is the total visible energy and $P_z^{vis} = \sum_j p_j^z$ stands for total longitudinal component of the visible momenta of the reconstructed objects. The above expression for $\sqrt{\hat{s}}_{\rm min}$ is obtained after minimizing the partonic Mandelstam variable $\hat{s}$ with respect to the invisible momenta subject to the missing transverse momentum constraints. This is a function extremization problem which can be done analytically as well as numerically, we have checked it numerically using Mathematica and found that the result exactly matches with the one mentioned in equation (4). It turns out that the first term depends on the visible decay products but the second term depends on the missing transverse energy $\not{E}_T$ and the sum of the invisible particle mass, m_{inv} after the minimization. Hence, the variable $\hat{s}_{\rm min}$ is a function of the sum of the masses of the invisible particles in the final state. However, fortunately, in our case the invisible particles are only neutrinos which makes $\hat{s}_{\rm min}$ independent of m_{inv} and it only depends on the visible momenta and missing transverse energy. Figure 2, (right panel) shows the distribution of $\sqrt{\hat{s}}_{\rm min}$. Similar to the earlier case, the distribution in red corresponds to the signal for a U_1 vector LQ of mass 1 TeV. By construction, $\sqrt{\hat{s}}_{\rm min}$ peaks at the threshold for the pair production. Considering the pair production of U_1 as our signal, the peak at 2 TeV hence matches well with the theoretical expectation for the variable. Since the threshold for the backgrounds are much smaller compared to the signal, this variable is also a smart choice as far as reducing the SM backgrounds is concerned.

The (1 + 2) dimensional transverse mass variable, M_{T2} [85–94], plays a pivotal role in reducing the background events. As a result, the signal significance is satisfactorily enhanced even though this variable was initially defined for the mass measurement of new particles both in long and short decay chains. The kinematic variable M_{T2} is defined as the maximum

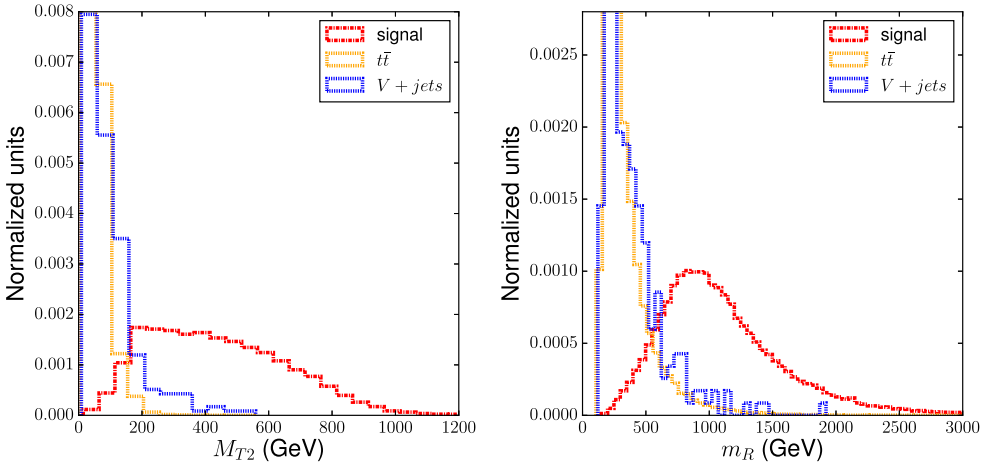

Figure 3. The variables M_{T2} (left panel) and m_R (right panel) are displayed where the red coloured histogram corresponds to the signal for a U_1 vector LQ of mass 1 TeV. As discussed in the text, the endpoint corresponding to M_{T2} falls at $M_{U_1} = 1$ TeV and m_R peaks at M_{U_1}.

transverse mass between the two parents satisfying the missing transverse momenta ($\vec{\not{p}}_T$) constraints and then minimizing over the momenta of the invisible particles (e.g. neutrino)

$$M_{T2}(m_\nu) \equiv \min_{\substack{\vec{q}_{iT} \\ \sum \vec{q}_{iT} = \vec{\not{p}}_T}} \left[\max_{i=1,2} \{ M_T^{(i)}(p_{iT}, q_{iT}, m_{vis(i)}; m_\nu) \} \right], \tag{5}$$

where the $M_T^{(i)}$ for each decay chain are

$$(M_T^{(i)})^2 = m_{vis(i)}^2 + m_\nu^2 + 2(E_T^{vis(i)} E_T^{\nu(i)} - \vec{p}_{iT}.\vec{q}_{iT}), \tag{6}$$

$$E_T^{vis(i)} = \sqrt{m_{vis(i)}^2 + p_{iT}^2}, \quad E_T^{\nu(i)} = \sqrt{m_\nu^2 + q_{iT}^2}. \tag{7}$$

In the above $\vec{p}_{iT}$ and $\vec{q}_{iT}$, $E_T^{vis(i)}$ and $E_T^{\nu(i)}$ are the transverse momentum, transverse energy of the large radius jet from top (anti-top) and neutrino, respectively. Note that the visible quantities in each event for the signal, are the two hardest P_T large radius jets (hardest P_T jets). The remaining reconstructed quantities are assumed to be soft and do not change the M_{T2} distribution significantly. Note that the minimization, in the definition of M_{T2}, acts over all the partitions of missing transverse momenta constraints. The maximization, on the other hand, is done between the two transverse masses for each partition. This ensures that the resulting M_{T2} gets closer to the U_1 mass, M_{U_1}. By construction, $M_{T2} \leqslant M_{U_1}$ where the equality holds when the top (anti-top) quark and the anti-neutrino (neutrino) are produced with equal rapidity. Hence, for the correct input mass of the invisible daughter particle, the endpoint for M_{T2} is at the mass of the U_1 vector LQ M_{U_1}. The neutrino mass being very small, we assume it to be zero for the M_{T2} calculation. In figure 3, (left panel) the M_{T2} distribution is displayed where the red colour corresponds to the signal. Since the mass of the U_1 vector LQ is taken to be 1 TeV, the end-point of the distribution, as expected, is at the same value albeit with very small number of events. Most of the backgrounds fall sharply at around 200 GeV which makes this mass bound variable extremely important in maximizing the signal to background ratio. The razor variable [101–104] is another interesting observable well known for handling

SM backgrounds with di-jet[7] and missing transverse energy produced from the pair production of heavy resonance. Assuming the heavy resonances are produced at the threshold, which is true for many BSM scenarios except the cases when the resonance is not so heavy, one calculates the two following mass variables:

$$m_R = \sqrt{(|\vec{p}_{j1}| + |\vec{p}_{j2}|)^2 - (p^z_{j1} + p^z_{j1})^2}\,, \tag{8}$$

$$m_{TR} = \sqrt{\frac{1}{2}[|\vec{\not{P}}_T|(p_T^{j1} + p_T^{j2}) - \vec{\not{P}}_T.(\vec{p}_T^{\,j1} + \vec{p}_T^{\,j2})]}\,. \tag{9}$$

In the razor frame, the longitudinal component of the momentum of the two visible decay products are equal and opposite. With this assumption, the variable m_R will display a peak at the mass of the U_1 vector LQ, M_{U_1} (where the neutrino mass is assumed to be zero). The transverse mass, m_{TR}, contains the information of the missing transverse energy due to neutrinos for signal events. The missing transverse energy for most of the background events is due to mismeasurement. Although, there are some background events which contain neutrino(s) in the final state, the number of events with such a final state is very small statistically and does not contribute much. Intuitively for the signal events transverse mass (m_{TR}) is smaller or equal to the U_1 vector LQ mass (M_{U_1}), i.e. $m_{TR} \leqslant M_{U_1}$, but such a relation will not hold for the background events. In order to better discriminate the signal and background events a dimensionless ratio is defined as follows

$$R \equiv \frac{m_{TR}}{m_R}. \tag{10}$$

While R for backgrounds will peak at zero, for the signal it will peak at higher values giving a better discrimination between the two. The variable m_R is represented in figure 3 (right panel). It is immediately evident that it peaks at the mass of the U_1 vector LQ for the signal events. The corresponding peak for backgrounds is at comparatively smaller values. The dimensionless ratio R is displayed in figure 4 which represents a 2 dimensional histogram where the colour axis represents the normalized events. The variable m_R along with the dimensionless ratio R is appropriate for handling the background events efficiently. Since the signal peaks at higher values of R and m_R in the $R - m_R$ plane compared to the backgrounds, a moderate cut on both R and m_R would be sufficient in order to minimize the backgrounds.

In addition to the above kinematic observables, there are some global and inclusive variables like the previously discussed $\sqrt{\hat{s}}_{\rm min}$ but independent of any parameter related to the invisible particle. Out of many similar observables from the literature which are extensively utilized in experimental analyses we have considered two of them, H_T [105] and $M_{\rm eff}$ [106]. The variable H_T is defined as the scalar sum of the transverse momenta of the visible decay products in the final state. In this analysis there only jets which are visible, so we have constructed H_T by doing the scalar sum of the transverse momentum of the jets. This is an inclusive variable which means it is unaffected by the combinatorial ambiguity of jets. It was proposed to give the information about the mass scale of new physics where there are large number of jets present in the final state. The variable $M_{\rm eff}$ is defined as the scalar sum of transverse momenta of jets and missing transverse energy, $M_{\rm eff} = \sum_i P_T^i(j) + \not{E}_T$. This variable also measures the mass scale of NP when there are invisible particles associated with it.

[7] In this analysis we have selected events with at least two large radius jets to calculate the razor variables for both the signal and backgrounds. For more than two large radius jets we select the two which are the hardest.

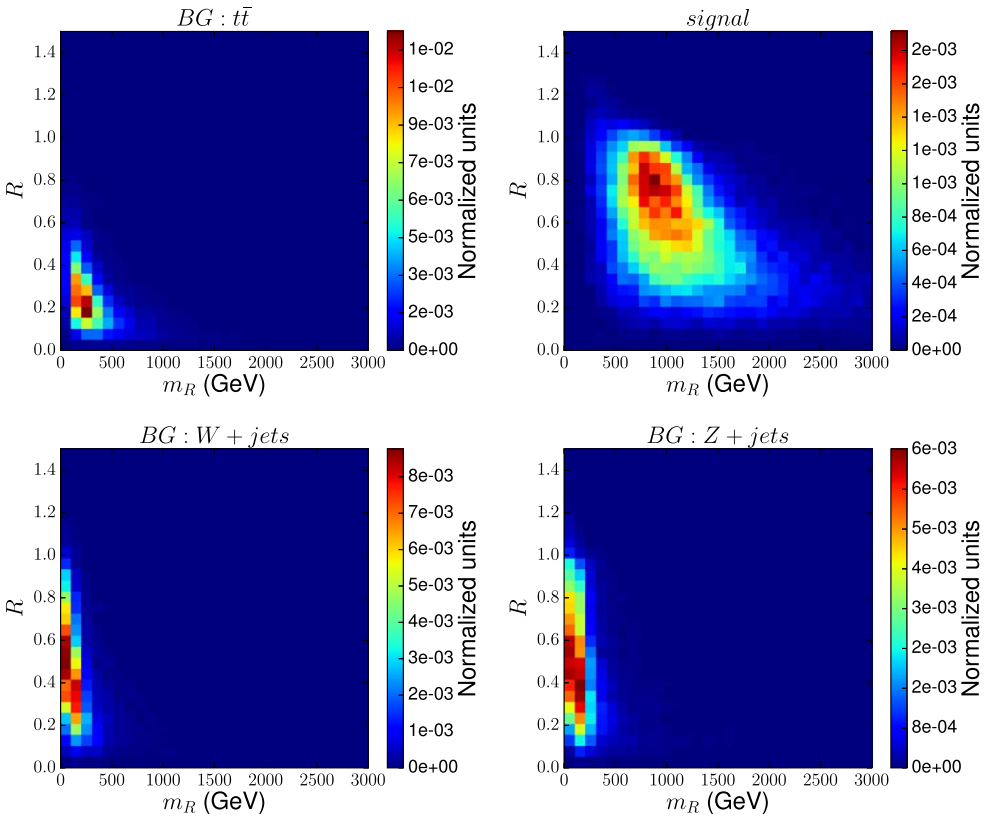

Figure 4. The dimensionless ratio of razor variables, R, in the y-axis and m_R in the x-axis with normalized events in the coloured bar represented for the signal and for the dominant backgrounds. By construction, as discussed in the text, the variable R peaks at higher values for the signal and for the backgrounds however, it peaks near zero. The variables R and m_R are very effective in distinguishing the signal from the background events.

We disentangle the signal and background by multivariate technique using toolkit for Multivariate data analysis (TMVA) with `Root`, particularly Boosted Decision Tree (BDT). We utilize the above discussed (efficient) variables along with some other interesting exclusive variable to maximize the signal significance. The following feature vectors are employed as input to BDT: $\not{E}_T$, H_T, $M_{\rm eff}$, $\sqrt{\hat{s}}_{\rm min}$, M_{T2}, M_R, R, N_b, N_{fatJet} and N_j. Where, the variables N_b and N_j are defined as the number of b−jets and number of jets respectively present in each event. The BDT response is displayed in figure 5 (left panel) where the red histogram corresponds to background events and the blue filled histogram is for the signal. Evidently, the signal and background distributions are well separated which in turn maximizes the LHC reach for the U_1 vector LQ. The signal and background events are calculated after putting an optimal BDT cut value, we have then enumerated the statistical significance of the aforementioned signal using the following formula:

$$\mathcal{S} = \frac{N_s}{\sqrt{N_s + N_b(1 + \epsilon_b)}}. \tag{11}$$

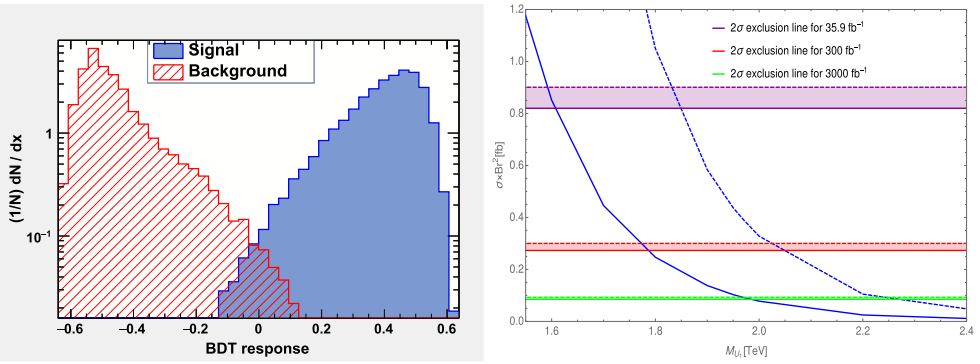

Figure 5. The figure (left panel) displays the BDT response for the considered signal (solid blue region) and background (red dashed region). As evident from the figure, BDT disentangles the signal from background quite efficiently. The exclusion limit (right panel) at 95% C.L. for the 13 TeV CM energy is presented for the signal. The exclusion limits are calculated for luminosities 35.9 fb^{-1} (purple band), 300 fb^{-1} (red band) and 3000 fb^{-1} (green band), respectively. The corresponding bands represent 20% systematic uncertainty in the background events. The dashed and solid blue lines represent the theoretical cross section times branching ratio square that are computed for 100% and 50% branching ratio of the vector LQ ($U_1 \rightarrow t\ \bar{\nu}$), respectively.

Here, $N_s(N_b)$ denotes the number of signal (background) events after implementing the BDT cut value for a specific luminosity and ϵ_b is systematic uncertainty [107]. The TMVA analysis gives background and signal cut efficiency as output for any given cut value of the method (here we have used BDT). It is then quite straight forward to calculate the number of signal (N_s) and background events (N_b) using corresponding cut efficiency and then the significance from equation (11). Using equation (11), we obtained a marginally improved expected limit of 1600 GeV for 13 TeV LHC with 35.9 fb^{-1} integrated luminosity (L_{int}) compared to the CMS analysis [47] where the observed (expected) exclusion limit at 95% C.L. was 1530 (1460) GeV. We find that the vector LQ can be excluded up to 1780 (1980) GeV at 95% C.L. for 13 TeV LHC with 300 (3000) fb^{-1} integrated luminosity. The above limits were computed for the vector LQ decaying to di-top plus missing energy channel with a 50% branching ratio. The LHC reach at 95% C.L. with 100% branching ratio are 1830, 2020 and 2230 GeV for 35.9, 300 and 3000 fb^{-1} integrated luminosity, respectively. In figure 5 (right panel) we depict the exclusion limit at 95% C.L. for $\sqrt{s} = 13$ TeV. The red and green bands denote the exclusion limits for 300 and 3000 fb^{-1} integrated luminosity, respectively. The blue solid (dashed) line denotes the effective theoretical production cross-section for 50% (100%) branching ratio, at the leading order, with the variation of the mass of U_1 vector LQ. The LHC reach for scalar LQ (see lower panel of figure no. 3 of [47]) decaying to the same channel, di-top plus missing energy, with 100% branching ratio at 13 TeV LHC is 1020 GeV for 35.9 fb^{-1} integrated luminosity. Evidently, the stronger LHC reach for the U_1vector LQ is mainly because of the higher production cross section compared to scalar leptoquark. Although, the choice $\kappa = 0$ and with 50% branching ratio will reduce the LHC limit for the vector LQ because of slightly smaller cross section but still larger than scalar LQ pair production. Hence, the vector LQ LHC reach may always be stronger than that of the scalar LQ for pair production in di-top plus missing energy channel. In addition, we have also taken 20% systematic uncertainty in the background estimation and calculated the significance. After the inclusion of systematic uncertainty, the significance is reduced slightly which can be seen

from the bands (purple, red and green for 35.9, 300 and 3000 fb^{-1} integrated luminosity, respectively) in right panel of figure 5. The mass of U_1 vector LQ can now be excluded up to 1585 GeV at 95% C.L. for 13 TeV LHC with 35.9 fb^{-1} integrated luminosity when the LQ decays to di-top plus missing energy channel with 50% branching ratio. This limit can reach up to 1770 and 1975 GeV for 300 and 3000 fb^{-1} integrated luminosity, respectively.

4. Constraints from $b \to c\tau\nu_l$ observables

Flavour physics has been instrumental in the search for NP which has been the main interest of the current phenomenological community for the last decade. The $\mathcal{R}_{D^{(*)}}$ and $\mathcal{R}_{K^{(*)}}$ ratios with deviations of about 3.08σ and 2.6σ from their SM values, respectively, along with other observables, have been much discussed as probes for such LFUV NP. However, since the U_1 vector LQ has been assumed to couple to third generation leptons, it will not contribute to the $\mathcal{R}_{K^{(*)}}$ anomalies. Hence, we carry out an analysis on the scope of the U_1 LQ in explaining the current $\mathcal{R}_{D^{(*)}}$ anomaly. Furthermore, in the case of $\mathcal{R}_{D^{(*)}}$ observable, due to the above mentioned assumption the NP couple only to the numerator (i.e. to the third generation leptons) while the denominator stays SM like. This approach has been widely followed in the community and is also the one that we follow in the flavor section of our analysis. We consider the data due to the different collaborations as separate data points instead of using the global average for these results. This results in an increase of statistics and degrees of freedom. It also allows us to take care of correlations unaccounted for in the global average, such as that between the 2016 and 2017 Belle measurement and the D^* polarization $P_\tau(D^*)$. We perform a fit to a total of 11 observables, including the fraction of the longitudinal polarization of $D^{(*)}$ ($F_L(D^*)$), the τ polarization in a $B \to D^*$ decay ($P_\tau(D^*)$) and the most recent Belle $\mathcal{R}_{D^{(*)}}$ measurements[8]. The observables we use in our fit are listed in table 1. The corresponding SM estimates are also mentioned on the topmost row, whereas the estimates for the U_1 vector LQ model are provided in the bottom row of the same table.

The effective Lagrangian for a $b \to c\tau\nu_l$ decay with all possible vector and scalar Wilson coefficients (WCs) with left-handed neutrinos can be written as [57]:

$$H_{\text{eff}} = \frac{4G_F}{\sqrt{2}} V_{cb}[(\delta_{l\tau} + C_{V_1}^l)\mathcal{O}_{V_1}^l + C_{V_2}^l \mathcal{O}_{V_2}^l + C_{S_1}^l \mathcal{O}_{S_1}^l + C_{S_2}^l \mathcal{O}_{S_2}^l + C_T^l \mathcal{O}_T^l], \tag{12}$$

where G_F is the Fermi constant for weak interactions, V_{cb} is the relevant Cabibbo–Kobayashi–Maskawa (CKM) element for $b \to c$ quark transitions. The U_1 vector LQ does not contribute to all of the above mentioned WCs, but only to $C_{V_1}^l$ and $C_{S_1}^l$. In accordance with [57] which provides the complete list of WCs relevant for LQ models and contributing to $b \to c\tau\nu$ decays and the corresponding operator basis, the $b \to c\tau\nu_l$ WCs relevant for the U_1 vector LQ can be written as[9]:

[8] We refrain from using the $R_{J/\psi}$ measurements since the corresponding SM estimates are far from accurate due to the absence of a reliable form factor parameterization for these decays.

[9] Our notation for the LQ couplings are slightly different from the one generally used in the literature. For example, h_{1L}^{cl} is generally written as h_{1L}^{2l} where the 1 in the superscript represents quarks from the second generation. However, for $l = \mu$, the second term in the numerator of $C_{V_1}^l$ is generally written as h_{1L}^{k2} but this time the number 2 represents first generation leptons. To avoid such confusions, we label the couplings using letters corresponding to the various quark and lepton generations where $l = e, \mu, \tau$

Table 1. Present status (both theoretical and experimental) of $\mathcal{R}(D)$, $\mathcal{R}(D^*)$, $P_\tau(D^*)$ and $F_L(D^*)$. First uncertainty is statistical and the second one is systematic. The first row lists the SM calculation obtained in this paper, while the last row includes the estimates for the U_1 vector LQ model after the fit.

	$\mathcal{R}(D)$	$\mathcal{R}(D^*)$	Correlation	$P_\tau(D^*)$	$F_L(D^*)$
SM	0.305(3)	0.260(9)		−0.486(29)	0.459(11)
Babar [48, 49]	$0.440(58)_{st.}(42)_{sy.}$	$0.332(24)_{st.}(18)_{sy.}$	−0.31		
Belle (2015) [51]	$0.375(64)_{st.}(26)_{sy.}$	$0.293(38)_{st.}(15)_{sy.}$	−0.50		
Belle (2016) [53, 108]	—	$0.270(35)_{st.}{}^{+0.028}_{-0.025}$	0.33	$-0.38(51)_{st.}{}^{+0.21}_{-0.16}$	
Belle (2019) [75]	$0.307(37)_{st.}(16)_{sy.}$	$0.283(18)_{st.}(14)_{sy.}$	−0.51		
LHCb (2015) [50]	—	$0.336(27)_{st.}(30)_{sy.}$			
LHCb (2017) [109, 110]	—	$0.280(18)_{st.}(29)_{sy.}$			
World avg. [111]	$0.340(27)_{st.}(13)_{sy.}$	$0.295(11)_{st.}(8)_{sy.}$	−0.38	$-0.38(51)_{st.}{}^{+0.21}_{-0.16}$	$0.60(08)_{st.}(035)_{sy.}$
U_1 vector LQ values.	0.347(51)	0.297(20)		−0.486(25)	0.459(12)

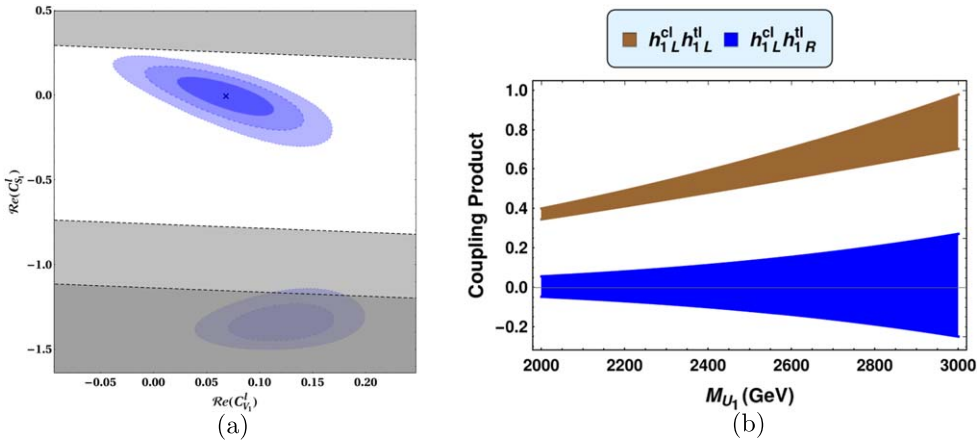

Figure 6. Our fit results displayed in the $\mathcal{R}e(C_{S_1}^{\ell})$ versus $\mathcal{R}e(C_{V_1}^{\ell})$ plane (figure 6(a)). One can see that there are two best fit regions. One of them is discarded by both the relaxed Br($B_c \leqslant 30\%$) [113] (shown in dark grey) and the aggressive Br($B_c \leqslant 10\%$) [114] (displayed in light grey) bounds. The best fit point is marked by a cross and the 1, 2 and 3σ contours corresponding to the best fit points are shown. The 1σ contour translates to the 1σ bands for the coupling products $h_{1L}^{cl} h_{1L}^{kl}$ and $h_{1L}^{cl} h_{1R}^{kl}$ in the model parameter space, displayed in brown and blue, respectively, in figure 6(b). Here $l = \tau$. The range for the mass of the U_1 vector LQ (the x-axis in figure 6(b)) is in accordance with the findings from the collider section of this work (see the last line of the second last paragraph under Introduction (section 1)).

$$C_{V_1}^{l} = \frac{1}{2\sqrt{2}\,G_F V_{cb}} \sum_{k=1}^{3} V_{k3} \frac{h_{1L}^{cl} h_{1L}^{kl}}{M_{U_1^{2/3}}^2},$$
$$C_{S_1}^{l} = -\frac{1}{2\sqrt{2}\,G_F V_{cb}} \sum_{k=1}^{3} V_{k3} \frac{2 h_{1L}^{cl} h_{1R}^{kl}}{M_{U_1^{2/3}}^2}, \tag{13}$$

where $l = e$, μ, τ in general, V_{k3} denotes the CKM elements and the upper index of the LQ denotes its electric charge. We discard the contribution from the Cabibbo suppressed terms and keep the leading terms proportional to $V_{33} = V_{tb}$.

The theoretical expressions for the observables $\mathcal{R}(D^{(*)})$ and the τ polarization $P_\tau(D^*)$ have been obtained from [57], and for the fraction of the longitudinal polarization of the D^* meson $F_L(D^*)$ from [112]. These expressions depend on the partial q^2 dependent decay widths for the $B \to D^{(*)} \tau \nu_l$ decays, where q^2 is the di-lepton invariant mass. These widths have also been taken from [57] and, for the sake of completion, have been provided in the appendix. In order to maintain parity with the collider section, we assume the WCs to be real. We also assume the U_1 vector LQ to couple to only the third generation leptons, and hence $l = \tau$ in the following.

The results from our fits are displayed in figure 6(a). One can see that there are two best-fit regions. However, one of them is discarded by the constraints due to the not yet measured branching ratio (Br) for the $B_c \to \tau\nu$ mode. It has been well known in the literature that pure scalar NP as an explanation for the $b \to c\tau\nu$ anomalies is highly constrained due to even a relaxed limit of $B_c \to \tau\nu \leqslant 30\%$ [113]. In our current analysis, we use this relaxed as well as a more aggressive bound of Br($B_c \to \tau\nu$) $\leqslant 10\%$ obtained from the LEP data taken at the Z-peak [114]. We see that both these constraints amount to one of the two best-fit regions

Table 2. The fit results for the NP parameters along with their 1σ errors. Here $l = \tau$.

Parameters	Fit values
$C_{V_1}^l$	0.068 ± 0.03
$C_{S_1}^l$	$-0.0019^{+0.0806}_{-0.0844}$

being discarded. The best-fit points that survive this constraint along with the corresponding 1σ errors are shown in table 2 [10]. This 1σ region translates into the 1σ bands in the model-parameter space for the U_1 vector LQ depicted in figure 6(b).

From figure 6(b) as well as table 2, it is clear that $C_{S_1}^l$ is consistent with its SM value of 0. This is primarily due to the fact that the inclusion of the most recent Belle (2019) results shifts the global average closer to the SM estimates for the $\mathcal{R}_{D^{(*)}}$ ratios, bringing the global deviation between the SM and the experimental results down from ~ 4 to $\sim 3\sigma$. The non-zero C_{V_1} is enough to explain such deviations in the $\mathcal{R}_{D^{(*)}}$ ratios. However, a glimpse at table 1 shows that the NP estimates corresponding to the $P_\tau(D^*)$ and the $F_L(D^*)$ observables for the U_1 vector LQ model are consistent with the corresponding SM estimates. While the NP estimates for $P_\tau(D^*)$ are also consistent with the corresponding experimental value within 1σ (primarily due to the large statistical error associated with its experimental value), the $F_L(D^*)$ NP estimate is off from its experimental value by almost 1.6σ.

5. Conclusion

In this article, we consider a particular type of leptoquark scenario that contains the U_1 leptoquark which conserves baryon and lepton numbers. This leptoquark mediates both charged as well as neutral current processes involved in the B-physics anomalies at tree level. In this work we have performed a comprehensive collider analysis of the U_1 vector leptoquark via multijet plus missing transverse energy final states. Further, in our current article we have assumed that the U_1 vector leptoquark couples with only third generation of leptons but with second and third generations of quarks, it will not contribute to the $b \to sll$ anomalies. We have hence studied the effect of such leptoquark in $b \to c$ observables only.

In addition, all the couplings share the same values. We have constructed several non-trivial kinematic variables which help us to reduce the SM background with respect to the signal in our collider analysis. We then implemented the interesting kinematic variables in a multivariate analysis, BDT, to maximize the LHC reach for the U_1 vector leptoquark. From our study, we have derived exclusion mass limits for the U_1 leptoquark at 95% C.L. corresponding to the 13 TeV LHC run with two benchmark values for integrated luminosities. For example, we can exclude up to 2020 (1780) GeV for an integrated luminosity of 300 fb^{-1}, 2230 (1980) GeV for 3000 fb^{-1} when the vector leptoquark decays with 100% (50%) branching ratio to the di-top plus missing energy channel.

We also analyse the scope of the U_1 leptoquark in explaining the $b \to c\tau\nu$ anomalies. We exclude the $R(J/\psi)$ data since the corresponding theoretical estimates are inaccurate, primarily due to lack of a proper form factor parameterization. We find that the U_1 leptoquark

[10] It should be mentioned here that a recent work [115, 116] disagrees with the 10% bound, claiming it to be too aggressive. They also argue that a more relaxed limit of 60% for the same branching ratio is allowed. However, in order to keep our analysis as aggressive as possible, we do not use the 60% limit. Using this limit will result in the discarded region being allowed, and will hence result in a more loosely constrained model parameter space. The values of the observables in the U_1 vector LQ model will, however, remain unchanged.

can potentially explain these results even after the more aggressive constraint of $\mathrm{Br}(B_c \leqslant \tau\nu)$ has been applied.

Acknowledgments

NG would like to acknowledge the Council of Scientific and Industrial Research (CSIR), Government of India for financial support. The work of AKS was supported by the Department of Science and Technology, Government of India under the fellowship reference number PDF/2017/002935 (SERB NPDF).

Appendix. $B \to D^{(*)}$ observables

The differential decay rate for $B \to D^{(*)}\tau\nu_l$ decays can be written as:

$$\begin{aligned}\frac{\mathrm{d}\Gamma(\overline{B} \to D\tau\overline{\nu}_l)}{\mathrm{d}q^2} &= \frac{G_F^2|V_{cb}|^2}{192\pi^3 m_B^3} q^2\sqrt{\lambda_D(q^2)}\left(1-\frac{m_\tau^2}{q^2}\right)^2 \\ &\times\Bigg\{|\delta_{l\tau}+C_{V_1}^l+C_{V_2}^l|^2\left[\left(1+\frac{m_\tau^2}{2q^2}\right)H_{V,0}^{s\,2}+\frac{3}{2}\frac{m_\tau^2}{q^2}H_{V,t}^{s\,2}\right] \\ &+\frac{3}{2}|C_{S_1}^l+C_{S_2}^l|^2\,H_S^{s\,2}+8|C_T^l|^2\left(1+\frac{2m_\tau^2}{q^2}\right)H_T^{s\,2} \\ &+3\Re[(\delta_{l\tau}+C_{V_1}^l+C_{V_2}^l)(C_{S_1}^{l*}+C_{S_2}^{l*})]\frac{m_\tau}{\sqrt{q^2}}H_S^s H_{V,t}^s \\ &-12\Re[(\delta_{l\tau}+C_{V_1}^l+C_{V_2}^l)C_T^{l*}]\frac{m_\tau}{\sqrt{q^2}}H_T^s H_{V,0}^s\Bigg\}, \end{aligned} \tag{-1}$$

and

$$\begin{aligned}\frac{\mathrm{d}\Gamma(\overline{B} \to D^*\tau\overline{\nu}_l)}{\mathrm{d}q^2} &= \frac{G_F^2|V_{cb}|^2}{192\pi^3 m_B^3} q^2\sqrt{\lambda_{D^*}(q^2)}\left(1-\frac{m_\tau^2}{q^2}\right)^2 \\ &\times\Bigg\{(|\delta_{l\tau}+C_{V_1}^l|^2+|C_{V_2}^l|^2)\left[\left(1+\frac{m_\tau^2}{2q^2}\right)(H_{V,+}^2+H_{V,-}^2+H_{V,0}^2)+\frac{3}{2}\frac{m_\tau^2}{q^2}H_{V,t}^2\right] \\ &-2\Re[(\delta_{l\tau}+C_{V_1}^l)C_{V_2}^{l*}]\left[\left(1+\frac{m_\tau^2}{2q^2}\right)(H_{V,0}^2+2H_{V,+}H_{V,-})+\frac{3}{2}\frac{m_\tau^2}{q^2}H_{V,t}^2\right] \\ &+\frac{3}{2}\,|C_{S_1}^l-C_{S_2}^l|^2\,H_S^2+8\,|C_T^l|^2\left(1+\frac{2m_\tau^2}{q^2}\right)(H_{T,+}^2+H_{T,-}^2+H_{T,0}^2) \\ &+3\Re[(\delta_{l\tau}+C_{V_1}^l-C_{V_2}^l)(C_{S_1}^{l*}-C_{S_2}^{l*})]\frac{m_\tau}{\sqrt{q^2}}H_S H_{V,t}-12\Re[(\delta_{l\tau} \\ &+C_{V_1}^l)C_T^{l*}]\frac{m_\tau}{\sqrt{q^2}}(H_{T,0}H_{V,0}+H_{T,+}H_{V,+}-H_{T,-}H_{V,-}) \\ &+12\Re[C_{V_2}^l C_T^{l*}]\frac{m_\tau}{\sqrt{q^2}}(H_{T,0}H_{V,0}+H_{T,+}H_{V,-}-H_{T,-}H_{V,+})\Bigg\}, \end{aligned} \tag{-2}$$

where $\lambda_{D^{(*)}}(q^2) = ((m_B - m_{D^{(*)}})^2 - q^2)((m_B + m_{D^{(*)}})^2 - q^2)$.

The τ polarization for a $B \to D^*$ decay ($P_\tau(D^*)$) is defined as:

$$P_\tau(D^*) = \frac{\Gamma(\lambda_\tau = 1/2) - \Gamma(\lambda_\tau = -1/2)}{\Gamma(\lambda_\tau = 1/2) + \Gamma(\lambda_\tau = -1/2)}, \tag{3}$$

where:

$$\begin{aligned}
\frac{\mathrm{d}\Gamma^{\lambda_\tau=1/2}(\overline{B} \to D^*\tau\overline{\nu}_l)}{\mathrm{d}q^2} &= \frac{G_F^2|V_{cb}|^2}{192\pi^3 m_B^3} q^2\sqrt{\lambda_{D^*}(q^2)}\left(1 - \frac{m_\tau^2}{q^2}\right)^2 \\
&\times \left\{\frac{1}{2}(|\delta_{l\tau} + C_{V_1}^l|^2 + |C_{V_2}^l|^2)\frac{m_\tau^2}{q^2}(H_{V,+}^2 + H_{V,-}^2 + H_{V,0}^2 + 3H_{V,t}^2)\right. \\
&- \Re[(\delta_{l\tau} + C_{V_1}^l)C_{V_2}^{l*}]\frac{m_\tau^2}{q^2}(H_{V,0}^2 + 2H_{V,+}H_{V,-} + 3H_{V,t}^2) \\
&+ \frac{3}{2}|C_{S_1}^l - C_{S_2}^l|^2\, H_S^2 + 8|C_T^l|^2(H_{T,+}^2 + H_{T,-}^2 + H_{T,0}^2) \\
&+ 3\Re[(\delta_{l\tau} + C_{V_1}^l - C_{V_2}^l)(C_{S_1}^{l*} - C_{S_2}^{l*})]\frac{m_\tau}{\sqrt{q^2}}\, H_S H_{V,t} \\
&- 4\Re[(\delta_{l\tau} + C_{V_1}^l)C_T^{l*}]\frac{m_\tau}{\sqrt{q^2}}(H_{T,0}H_{V,0} + H_{T,+}H_{V,+} - H_{T,-}H_{V,-}) \\
&\left.+ 4\Re[C_{V_2}^l C_T^{l*}]\frac{m_\tau}{\sqrt{q^2}}(H_{T,0}H_{V,0} + H_{T,+}H_{V,-} - H_{T,-}H_{V,+})\right\},
\end{aligned} \tag{4a}$$

$$\begin{aligned}
\frac{\mathrm{d}\Gamma^{\lambda_\tau=-1/2}(\overline{B} \to D^*\tau\overline{\nu}_l)}{\mathrm{d}q^2} &= \frac{G_F^2|V_{cb}|^2}{192\pi^3 m_B^3} q^2\sqrt{\lambda_{D^*}(q^2)}\left(1 - \frac{m_\tau^2}{q^2}\right)^2 \\
&\times \left\{(|\delta_{l\tau} + C_{V_1}^l|^2 + |C_{V_2}^l|^2)(H_{V,+}^2 + H_{V,-}^2 + H_{V,0}^2)\right. \\
&- 2\Re[(\delta_{l\tau} + C_{V_1}^l)C_{V_2}^{l*}](H_{V,0}^2 + 2H_{V,+}H_{V,-}) \\
&+ 16|C_T^l|^2\frac{m_\tau^2}{q^2}(H_{T,+}^2 + H_{T,-}^2 + H_{T,0}^2) \\
&- 8\Re[(\delta_{l\tau} + C_{V_1}^l)C_T^{l*}]\frac{m_\tau}{\sqrt{q^2}}(H_{T,0}H_{V,0} + H_{T,+}H_{V,+} - H_{T,-}H_{V,-}) \\
&\left.+ 8\Re[C_{V_2}^l C_T^{l*}]\frac{m_\tau}{\sqrt{q^2}}(H_{T,0}H_{V,0} + H_{T,+}H_{V,-} - H_{T,-}H_{V,+})\right\}.
\end{aligned} \tag{4b}$$

The D^* polarization $F_L(D^*)$ is defined as:

$$F_L(D^*) = \frac{\Gamma(\lambda_{D^*} = 0)}{\Gamma(\lambda_{D^*} = 0) + \Gamma(\lambda_{D^*} = 1) + \Gamma(\lambda_{D^*} = -1)}, \tag{5}$$

where:

$$\frac{\mathrm{d}\Gamma^{\lambda_{D^*}=\pm 1}(\overline{B} \to D^*\tau\overline{\nu}_l)}{\mathrm{d}q^2} = \frac{G_F^2|V_{cb}|^2}{192\pi^3 m_B^3} q^2\sqrt{\lambda_{D^*}(q^2)}\left(1-\frac{m_\tau^2}{q^2}\right)^2$$
$$\times\left\{\left(1+\frac{m_\tau^2}{2q^2}\right)(|\delta_{l\tau}+C_{V_1}^l|^2 H_{V,\pm}^2 + |C_{V_2}^l|^2 H_{V,\mp}^2\right.$$
$$-2\Re[(\delta_{l\tau}+C_{V_1}^l)C_{V_2}^{l*}]H_{V,+}H_{V,-}) + 8|C_T^l|^2\left(1+\frac{2m_\tau^2}{q^2}\right)H_{T,\pm}^2$$
$$\left.\mp 12\Re[(\delta_{l\tau}+C_{V_1}^l)C_T^{l*}]\frac{m_\tau}{\sqrt{q^2}}H_{T,\pm}H_{V,\pm} \pm 12\Re[C_{V_2}^l C_T^{l*}]\frac{m_\tau}{\sqrt{q^2}}H_{T,\pm}H_{V,\mp}\right\}, \tag{6a}$$

$$\frac{\mathrm{d}\Gamma^{\lambda_{D^*}=0}(\overline{B} \to D^*\tau\overline{\nu}_l)}{\mathrm{d}q^2} = \frac{G_F^2|V_{cb}|^2}{192\pi^3 m_B^3} q^2\sqrt{\lambda_{D^*}(q^2)}\left(1-\frac{m_\tau^2}{q^2}\right)^2$$
$$\times\left\{|\delta_{l\tau}+C_{V_1}^l-C_{V_2}^l|^2\left[\left(1+\frac{m_\tau^2}{2q^2}\right)H_{V,0}^2+\frac{3}{2}\frac{m_\tau^2}{q^2}H_{V,t}^2\right]\right.$$
$$+\frac{3}{2}|C_{S_1}^l-C_{S_2}^l|^2 H_S^2 + 8|C_T^l|^2\left(1+\frac{2m_\tau^2}{q^2}\right)H_{T,0}^2$$
$$+3\Re[(\delta_{l\tau}+C_{V_1}^l-C_{V_2}^l)(C_{S_1}^{l*}-C_{S_2}^{l*})]\frac{m_\tau}{\sqrt{q^2}}H_S H_{V,t} - 12\Re[(\delta_{l\tau}$$
$$\left.+C_{V_1}^l-C_{V_2}^l)C_T^{l*}]\frac{m_\tau}{\sqrt{q^2}}H_{T,0}H_{V,0}\right\}. \tag{6b}$$

In all the above, the H's are the so called helicity amplitudes which can be written down in terms of the corresponding hadronic form factor parameters. We refer to [57] for a detailed description of the same. In accordance with the same reference, we have used the Caprini–Lellouch–Neubert (CLN) [117] parametrization for the $B \to D^{(*)}$ form factors.

ORCID iDs

Avirup Shaw https://orcid.org/0000-0002-2359-3123
Abhaya Kumar Swain https://orcid.org/0000-0002-2291-0481

References

[1] Ruckl R, Wyler D and Buchmuller W 1987 Leptoquarks in Lepton–Quark Collisions *Phys. Lett.* B **191** 442–8
Buchmuller W, Ruckl R and Wyler D 1999 *Phys. Lett.* B **448** 320–320 (erratum)
[2] Schrempp B and Schrempp F 1985 Light leptoquarks *Phys. Lett.* B **153** 101–7
[3] Georgi H and Glashow S L 1974 Unity of all elementary particle forces *Phys. Rev. Lett.* **32** 438–41
[4] Pati J C and Salam A 1973 Is baryon number conserved? *Phys. Rev. Lett.* **31** 661–4
[5] Dimopoulos S and Susskind L 1979 Mass without scalars *Phys. Nucl.* B **155** 237–52
[6] Dimopoulos S 1980 Technicolored signatures *Nucl. Phys.* B **168** 69–92

[7] Langacker P 1981 Grand unified theories and proton decay *Phys. Rep.* **72** 185
[8] Senjanovic G and Sokorac A 1983 Light Leptoquarks in SO(10) *Z. Phys.* C **20** 255
[9] Cashmore R J *et al* 1985 Exotic phenomena in high-energy E P collisions *Phys. Rep.* **122** 275–386
[10] Pati J C and Salam A 1974 Lepton number as the fourth color *Phys. Rev.* D **10** 275–89
[11] Green M B and Schwarz J H 1984 Anomaly cancellation in supersymmetric $D = 10$ gauge theory and superstring theory *Phys. Lett.* B **149** 117–22
[12] Witten E 1985 Symmetry breaking patterns in superstring models *Nucl. Phys.* B **258** 75
[13] Gross D J, Harvey J A, Martinec E J and Rohm R 1985 The heterotic string *Phys. Rev. Lett.* **54** 502–5
[14] Hewett J L and Rizzo T G 1989 Low-energy phenomenology of superstring inspired E(6) models *Phys. Rep.* **183** 193
[15] Davidson S, Bailey D C and Campbell B A 1994 Model independent constraints on leptoquarks from rare processes *Z. Phys.* C **61** 613–44
[16] Hewett J L and Rizzo T G 1997 Much ado about leptoquarks: a comprehensive analysis *Phys. Rev.* D **56** 5709–24
[17] Nath P and Perez P Fileviez 2007 Proton stability in grand unified theories, in strings and in branes *Phys. Rep.* **441** 191–317
[18] Shanker O U 1982 Flavor violation, scalar particles and leptoquarks *Nucl. Phys.* B **206** 253–72
[19] Shanker O U 1982 $\pi\ell$ 2, $K\ell$ 3 and $K^0 - \bar{K}0$ Constraints on Leptoquarks and supersymmetric particles *Nucl. Phys.* B **204** 375–86
[20] Buchmuller W and Wyler D 1986 Constraints on SU(5) type leptoquarks *Phys. Lett.* B **177** 377–82
[21] Hewett J L and Pakvasa S 1988 Leptoquark production in hadron colliders *Phys. Rev.* D **37** 3165
[22] Leurer M 1994 A Comprehensive study of leptoquark bounds *Phys. Rev.* D **49** 333–42
[23] Leurer M 1994 Bounds on vector leptoquarks *Phys. Rev.* D **50** 536–41
[24] Dorsner I, Fajfer S and Greljo A 2014 Cornering scalar leptoquarks at LHC *J. High Energy Phys.* **10** 154
[25] Allanach B, Alves A, Queiroz F S, Sinha K and Strumia A 2015 Interpreting the CMS $\ell^+\ell^- jj\not{E}_{\mathrm{T}}$ excess with a leptoquark model *Phys. Rev.* D **92** 055023
[26] Evans J L and Nagata N 2015 Signatures of leptoquarks at the LHC and right-handed neutrinos *Phys. Rev.* D **92** 015022
[27] Li X-Q, Yang Y-D and Zhang X 2016 Revisiting the one leptoquark solution to the R(D $^{(*)}$) anomalies and its phenomenological implications *J. High Energy Phys.* **08** 054
[28] Diaz B, Schmaltz M and Zhong Y-M 2017 The leptoquark hunteras guide: pair production *J. High Energy Phys.* **10** 097
[29] Dumont B, Nishiwaki K and Watanabe R 2016 LHC constraints and prospects for S_1 scalar leptoquark explaining the $\bar{B} \to D^{(*)}\tau\bar{\nu}$ anomaly *Phys. Rev.* D **94** 034001
[30] Faroughy D A, Greljo A and Kamenik J F 2017 Confronting lepton flavor universality violation in B decays with high-p_T tau lepton searches at LHC *Phys. Lett.* B **764** 126–34
[31] Greljo A and Marzocca D 2017 High-p_T dilepton tails and flavor physics *Eur. Phys. J.* C **77** 548
[32] Doršner I, Fajfer S, Faroughy D A and Košnik N 2017 The role of the S_3 GUT leptoquark in flavor universality and collider searches *J. High Energ. Phys.* **2017** 188
[33] Allanach B C, Gripaios B and You T 2018 The case for future hadron colliders from $B \to K^{(*)}\mu^+\mu^-$ decays *J. High Energy Phys.* **03** 021
[34] Crivellin A, Müller D and Ota T 2017 Simultaneous explanation of $R(D^{()})$ and bs^+: the last scalar leptoquarks standing *J. High Energy Phys.* **09** 040
[35] Hiller G and Nisandzic I 2017 R_K and R_{K^*} beyond the standard model *Phys. Rev.* D **96** 035003
[36] Buttazzo D, Greljo A, Isidori G and Marzocca D 2017 B-physics anomalies: a guide to combined explanations *J. High Energy Phys.* **11** 044
[37] Calibbi L, Crivellin A and Li T 2018 A model of vector leptoquarks in view of the *B*-physics anomalies *Phys. Rev.* D **98** 115002
[38] Sahoo S, Mohanta R and Giri A K 2017 Explaining the R_K and $R_{D^{(*)}}$ anomalies with vector leptoquarks *Phys. Rev.* D **95** 035027
[39] Altmannshofer W, Bhupal Dev P and Soni A 2017 *Phys. Rev.* D **96** 095010
[40] Baumgartel D and (CMS collaboration) 2014 Searches for the pair production of scalar leptoquarks at CMS *J. Phys.: Conf. Ser.* **485** 012053

[41] Aad G *et al* (ATLAS collaboration) 2016 Searches for scalar leptoquarks in pp collisions at $\sqrt{s} = 8$ TeV with the ATLAS detector *Eur. Phys. J.* C **76** 5

[42] Aaboud M *et al* (ATLAS collaboration) 2016 Search for scalar leptoquarks in pp collisions at $\sqrt{s} = 13$ TeV with the ATLAS experiment *New J. Phys.* **18** 093016

[43] Sirunyan A M *et al* (CMS collaboration) 2017 Search for third-generation scalar leptoquarks and heavy right-handed neutrinos in final states with two tau leptons and two jets in proton–proton collisions at $\sqrt{s} = 13$ TeV *J. High Energy Phys.* **07** 121

[44] Sirunyan A M (CMS collaboration) *et al* 2018 Search for third-generation scalar leptoquarks decaying to a top quark and a τ lepton at $\sqrt{s} = 13$ TeV *Eur. Phys. J.* C **78** 707

[45] Aaltonen T *et al* (CDF collaboration) 2008 Search for third generation Vector Leptoquarks in $p\bar{p}$ collisions at $\sqrt{s} = 1.96$ TeV *Phys. Rev.* D **77** 091105

[46] Sirunyan A M *et al* (CMS collaboration) 2018 Search for leptoquarks coupled to third-generation quarks in proton-proton collisions at $\sqrt{s} = 13$ TeV *Phys. Rev. Lett.* **121** 241802

[47] Sirunyan A M *et al* (CMS collaboration) 2018 *Phys. Rev.* D **98** 032005

[48] Lees J P *et al* (BaBar collaboration) 2012 Evidence for an excess of $\bar{B} \to D^{(*)}\tau^-\bar{\nu}_\tau$ decays *Phys. Rev. Lett.* **109** 101802

[49] Lees J P and (BaBar collaboration) 2013 Measurement of an excess of $\bar{B} \to D^{(*)}\tau^-\bar{\nu}_\tau$ decays and implications for charged Higgs bosons *Phys. Rev.* D **88** 072012

[50] Aaij R *et al* (LHCb collaboration) 2015 *Phys. Rev. Lett.* **115** 111803

[51] Huschle M *et al* (Belle collaboration) 2015 Measurement of the branching ratio of $\bar{B} \to D^{(*)}\tau^-\bar{\nu}_\tau$ relative to $\bar{B} \to D^{(*)}\ell^-\bar{\nu}_\ell$ decays with hadronic tagging at Belle *Phys. Rev.* D **92** 072014

[52] Sato Y *et al* (Belle collaboration) 2016 Measurement of the branching ratio of $\bar{B}^0 \to D^{*+}\tau^-\bar{\nu}_\tau$ relative to $\bar{B}^0 \to D^{*+}\ell^-\bar{\nu}_\ell$ decays with a semileptonic tagging method *Phys. Rev.* D **94** 072007

[53] Hirose S *et al* (Belle collaboration) 2017 Measurement of the τ lepton polarization and $R(D^*)$ in the decay $\bar{B} \to D^*\tau^-\bar{\nu}_\tau$ *Phys. Rev. Lett.* **118** 211801

[54] Aaij R *et al* (LHCb collaboration) 2014 Test of lepton universality using $B^+ \to K^+\ell^+\ell^-$ decays *Phys. Rev. Lett.* **113** 151601

[55] Aaij R *et al* (LHCb collaboration) 2016 Angular analysis of the $B^0 \to K^{*0}\mu^+\mu^-$ decay using 3 fb^{-1} of integrated luminosity *J. High Energy Phys.* **02** 104

[56] Aaij R *et al* (LHCb collaboration) 2017 Test of lepton universality with $B^0 \to K^{*0}\ell^+\ell^-$ decays *J. High Energy Phys.* **08** 055

[57] Sakaki Y, Tanaka M, Tayduganov A and Watanabe R 2013 Testing leptoquark models in $\bar{B} \to D^{(*)}\tau\bar{\nu}$ *Phys. Rev.* D **88** 094012

[58] Popov O and White G A 2017 One Leptoquark to unify them? Neutrino masses and unification in the light of $(g-2)_\mu$, $R_{D^{(*)}}$ and R_K anomalies *Nucl. Phys.* B **923** 324–38

[59] Chen C-H, Nomura T and Okada H 2017 Excesses of muon $g-2$, $R_{D^{(*)}}$, and R_K in a leptoquark model *Phys. Lett.* B 456–64

[60] Alok A K, Bhattacharya B, Datta A, Kumar D, Kumar J and London D 2017 New physics in $b \to s\mu^+\mu^-$ after the measurement of R_{K^*} *Phys. Rev.* D **96** 095009

[61] Assad N, Fornal B and Grinstein B 2018 Baryon number and lepton universality violation in leptoquark and diquark models *Phys. Lett.* B **777** 324–31

[62] Aloni D, Dery A, Frugiuele C and Nir Y 2017 Testing minimal flavor violation in leptoquark models of the $R_{K^{(*)}}$ anomaly *J. High Energy Phys.* **11** 109

[63] Wold I G B, Finkelstein S L, Barger A J, Cowie L L and Rosenwasser B 2017 *Astrophys. J.* **848** 108

[64] Müller D 2018 Leptoquarks in flavour physics *EPJ Web Conf.* **179** 01015

[65] Hiller G, Loose D and Nišandžić I 2018 Flavorful leptoquarks at hadron colliders *Phys. Rev.* D **97** 075004

[66] Biswas A, Ghosh D K, Patra S K and Shaw A 2019 Int. J. Mod. Phys. *Int. J. Mod. Phys.* A **34** 1950112

[67] Fajfer S, Košnik N and Vale Silva L 2018 Footprints of leptoquarks: from $R_{K^{(*)}}$ to $K \to \pi\nu\bar{\nu}$ *Eur. Phys. J.* C **78** 275

[68] Monteux A and Rajaraman A 2018 B anomalies and Leptoquarks at the LHC: beyond the Lepton–Quark final state *Phys. Rev.* D **98** 115032

[69] Kumar J, London D and Watanabe R 2019 Combined Explanations of the $b \to s\mu^+\mu^-$ and $b \to c\tau^-\bar{\nu}$ Anomalies: a General Model Analysis *Phys. Rev.* D **99** 015007

[70] Crivellin A, Greub C, Saturnino F and Müller D 2019 Importance of loop effects in explaining the accumulated evidence for New Physics in B decays with a Vector Leptoquark *Phys. Rev. Lett.* **122** 011805
[71] Bandyopadhyay P and Mandal R 2018 Revisiting scalar leptoquark at the LHC *Eur. Phys. J.* C **78** 491
[72] Vignaroli N 2019 Seeking leptoquarks in the $\mathbf{t\bar{t}}$ plus missing energy channel at the high-luminosity LHC *Phys. Rev.* D **99** 035021
[73] Doršner I and Greljo A 2018 Leptoquark toolbox for precision collider studies *J. High Energy Phys.* **05** 126
[74] Biswas A, Shaw A and Swain A K 2019 Collider signature of V_2 Leptoquark with $b \rightarrow s$ flavour observables *Lett. High Energy Phys.* **2** 126
[75] Abdesselam A(Belle collaboration) *et al Measurement of* $\mathcal{R}(D)$ *and* $\mathcal{R}(D^*)$ *with a Semileptonic Tagging Method* arXiv:1904.08794
[76] Doršner I, Fajfer S, Greljo A, Kamenik J F and Košnik N 2016 Physics of leptoquarks in precision experiments and at particle colliders *Phys. Rep.* **641** 1–68
[77] Alwall J *et al* 2014 The automated computation of tree-level and next-to-leading order differential cross sections, and their matching to parton shower simulations *J. High Energy Phys.* **07** 079
[78] Ball R D *et al* (NNPDF collaboration) 2015 Parton distributions for the LHC Run II *J. High Energy Phys.* **04** 040
[79] Alloul A, Christensen N D, Degrande C, Duhr C and Fuks B 2014 FeynRules 2.0—a complete toolbox for tree-level phenomenology *Comput. Phys. Commun.* **185** 2250–-2300
[80] Sjostrand T, Mrenna S and Skands P Z 2006 PYTHIA 6.4 Physics and Manual *J. High Energy Phys.* **05** 026
[81] de Favereau J *et al* (DELPHES 3) 2014 DELPHES 3, A modular framework for fast simulation of a generic collider experiment *J. High Energy Phys.* **02** 057
[82] Cacciari M, Salam G P and Soyez G 2012 FastJet user manual *Eur. Phys. J.* C **72** 1896
[83] Hoeche S *et al* 2005 Matching parton showers and matrix elements *HERA and the LHC: A Workshop on the implications of HERA for LHC physics: Proceedings Part A* 288–9
[84] Czakon M and Mitov A 2014 Top..: a program for the calculation of the top-pair cross-section at hadron colliders *Comput. Phys. Commun.* **185** 2930
[85] Lester C and Summers D 1999 Measuring masses of semiinvisibly decaying particles pair produced at hadron colliders *Phys. Lett.* B **463** 99–103
[86] Barr A, Lester C and Stephens P 2003 *J. Phys. G: Nucl. Part. Phys.* **29** 2343–63
[87] Meade P and Reece M 2006 Top partners at the LHC: Spin and mass measurement *Phys. Rev.* D **74** 015010
[88] Lester C and Barr A 2007 MTGEN: Mass scale measurements in pair-production at colliders *J. High Energy Phys.* **0712** 102
[89] Cho W S, Choi K, Kim Y G and Park C B 2008 *Phys. Rev. Lett.* **100** 171801
[90] Cho W S, Choi K, Kim Y G and Park C B 2008 Measuring superparticle masses at hadron collider using the transverse mass kink *J. High Energy Phys.* **0802** 035
[91] Barr A J, Gripaios B and Lester C G 2008 Weighing wimps with kinks at colliders: invisible particle mass measurements from endpoints *J. High Energy Phys.* **0802** 014
[92] Gripaios B 2008 Transverse observables and mass determination at hadron colliders *J. High Energy Phys.* **0802** 053
[93] Nojiri M M, Shimizu Y, Okada S and Kawagoe K 2008 Inclusive transverse mass analysis for squark and gluino mass determination *J. High Energy Phys.* **0806** 035
[94] Konar P, Kong K, Matchev K T and Park M 2010 Dark matter particle spectroscopy at the LHC: generalizing M(T2) to asymmetric event topologies *J. High Energy Phys.* **1004** 086
[95] Konar P, Kong K and Matchev K T 2009 $\sqrt{\hat{s}}_{\min}$: A Global inclusive variable for determining the mass scale of new physics in events with missing energy at hadron colliders *J. High Energy Phys.* **03** 085
[96] Konar P, Kong K, Matchev K T and Park M 2011 RECO level $\sqrt{s}_{\min}$ and subsystem $\sqrt{s}_{\min}$: Improved global inclusive variables for measuring the new physics mass scale in $\not{E}_T$ events at hadron colliders *J. High Energy Phys.* **06** 041
[97] Papaefstathiou A and Webber B 2009 Effects of QCD radiation on inclusive variables for determining the scale of new physics at hadron colliders *J. High Energy Phys.* **06** 069

[98] Papaefstathiou A and Webber B 2010 Effects of invisible particle emission on global inclusive variables at hadron colliders *J. High Energy Phys.* **07** 018
[99] Swain A K and Konar P 2015 Constrained $\sqrt{\hat{s}_{\min}}$ and reconstructing with semi-invisible production at hadron colliders *J. High Energy Phys.* **03** 142
[100] Swain A K and Konar P 2016 Mass determination and event reconstruction at Large Hadron Collider *Springer Proc. Phys.* **174** 599–603
[101] Rogan C Kinematical variables towards new dynamics at The LHC arXiv:1006.2727
[102] Buckley M R, Lykken J D, Rogan C and Spiropulu M 2014 Super-razor and searches for sleptons and charginos at the LHC *Phys. Rev.* D **89** 055020
[103] Chatrchyan S *et al* (CMS) 2012 Inclusive search for squarks and gluinos in *pp* collisions at $\sqrt{s} = 7$ TeV *Phys. Rev.* D **85**
[104] Khachatryan V *et al* (CMS) 2015 Search for supersymmetry using Razor variables in events with *b*-tagged jets in *pp* collisions at $\sqrt{s} = 8$ TeV *Phys. Rev.* D **91** 052018
[105] Tovey D R 2001 Measuring the SUSY mass scale at the LHC *Phys. Lett.* B **498** 1–10
[106] Hinchliffe I, Paige F E, Shapiro M D, Soderqvist J and Yao W 1997 *Phys. Rev.* D **55** 5520–40
[107] Cowan G 2012 Discovery sensitivity for a counting experiment with background uncertainty http://www.pp.rhul.ac.uk/cowan/stat/medsig/medsigNote.pdf
[108] Hirose S *et al* (Belle) 2018 Measurement of the τ lepton polarization and $R(D^*)$ in the decay $\bar{B} \to D^* \tau^- \bar{\nu}_\tau$ with one-prong hadronic τ decays at Belle *Phys. Rev.* D **97** 012004
[109] Aaij R *et al* (LHCb) 2018 Test of Lepton Flavor Universality by the measurement of the $B^0 \to D^{*-} \tau^+ \nu_\tau$ branching fraction using three-prong τ decays *Phys. Rev.* D **97** 072013
[110] Aaij R *et al* (LHCb) 2018 Measurement of the ratio of the $B^0 \to D^{*-} \tau^+ \nu_\tau$ and $B^0 \to D^{*-} \mu^+ \nu_\mu$ branching fractions using three-prong τ-lepton decays *Phys. Rev. Lett.* **120** 171802
[111] Adamczyk K and (Belle, Belle-II) 2019 *Semitauonic B decays at Belle/Belle II, in 10th International Workshop on the CKM Unitarity Triangle (CKM 2018) (Heidelberg, Germany, 17–21 September 2018)* arXiv:1901.06380
[112] Bhattacharya S, Nandi S and Patra S K 2019 $b \to c\tau\nu_\tau$ Decays: a catalogue to compare, constrain, and correlate new physics effects *Eur. Phys. J.* C **79** 268
[113] Alonso R, Grinstein B and Martin Camalich J 2017 Lifetime of B_c^- constrains explanations for anomalies in $B \to D^{(*)} \tau\nu$ *Phys. Rev. Lett.* **118** 081802
[114] Akeroyd A G and Chen C-H 2017 *Phys. Rev.* D **96** 075011
[115] Blanke M *et al* 2019 Impact of polarization observables and $B_c \to \tau\nu$ on new physics explanations of the $b \to c\tau\nu$ anomaly *Phys. Rev.* D **99** 075006
[116] Blanke M, Crivellin A, Kitahara T, Moscati M, Nierste U and Nišandžić I 2019 *Phys. Rev.* D **100** 035035
[117] Caprini I, Lellouch L and Neubert M 1998 Dispersive bounds on the shape of $\bar{B} \to D^{(*)} \ell\bar{\nu}$ form-factors *Nucl. Phys.* B **530** 153–81